https://doi.org/10.48048/tis.2023.6008

In silico Pharmacological Evaluation of Tetrahydro-β-carboline Derivatives as Putative Inhibitors of Alpha-Synuclein and Dopa Decarboxylase for Parkinson's Disease

Tham Xuan Yao[1], Yusuf Oloruntoyin Ayipo[2,3,*] and Mohd Nizam Mordi[2]

[1]*Department of Biomedical Sciences, Universiti Putra Malaysia, Serdang Lama 43400, Malaysia*
[2]*Centre for Drug Research, Universiti Sains Malaysia, Pulau Pinang 11800, Malaysia*
[3]*Department of Chemistry and Industrial Chemistry, Kwara State University, Kwara 241103, Nigeria*

([*]Corresponding author's e-mail: yusuf.ayipo@kwasu.edu.ng)

Received: 18 September 2022, Revised: 22 October 2022, Accepted: 29 October 2022, Published: 28 August 2023

Abstract

Parkinson's disease (PD) is a neurological problem that results mostly in disability globally due to therapeutic challenges. Alpha-synuclein (ASN) and Dopa decarboxylase (DDC) are strongly implicated in the pathogenesis of PD including the aggregation of Lewy bodies and degeneration of dopamine-producing cells. These make them plausible drug targets commonly explored by researchers in the quest for potent inhibitors. However, up to this moment, no inhibitor of ASN has been approved for clinical application while only a handful is available for DDC, as such, searching for effective inhibitors of the dual targets remains essential. In this study, the in-house databases of tetrahydro-β-carboline and carbazole derivatives were virtually screened for putative ligands with multitarget inhibitory mechanisms against the ASN and DDC using molecular docking protocols. Relevant drugs such as phenylbutyrate, anle138b, levodopa, carbidopa and benserazide were used as references. The physicochemical, pharmacokinetics, pharmacodynamics and toxicological profiles of the selected ligands and references were also evaluated *in silico* using pkCSM. From the virtual screening, ligands 172, 082 and 013 interacted more strongly with ASN receptors with SP glide gscores of –9.154, –9.124 and –8.971 kcal/mol respectively as compared to phenylbutyrate and anle138b with SP glide gscores of –7.181 and –5.875 kcal/mol. They also showed higher binding affinities to DDC receptor by higher SP glide gscores of –6.758, –5.212 and –6.271 kcal/mol than levodopa, carbidopa and benserazide with values of –4.217, –4.502 and –4.18 kcal/mol respectively. Among the 3 ligands, ligand 172 satisfies Lipinski's Rules of 5 (RO5) and demonstrates ADMET parameters that favor a central nervous system (CNS) drug which was identified as potent inhibitors of ASN and DDC responsible for PD. The potential ligands with stronger inhibitory interactions and good ADMET profile are amenable for further experimental validation in the quest for potent inhibitors of ASN and DDC as anti-PD agents.

Keywords: Parkinson's disease, Alpha-synuclein, Dopa decarboxylase, Lewy bodies, Molecular docking, *In silico* ADMET, β-carboline alkaloids, Central nervous system

Introduction

PD is a progressive neurodegenerative disorder that is caused by the loss of dopamine-producing cells in the substantia nigra of the midbrain [1]. Common symptoms of PD include rigidity, resting tremors, bradykinesia, impaired motor coordination and instability in posture [2]. Among all the neurological disorders, PD has the fastest increase in prevalence with its high resultant in disability and deaths worldwide. It is being shown that in year 2016, 6.1 million people were reportedly affected by PD globally with 21.7 % increase in prevalence rate according to specified age groups within 26 years from year 1990 [3]. However, at present, no cure has been found for PD, though, there are a variety of drugs that can help to relieve the symptoms. ASN and DDC have attracted the attention of most researchers due to their relevance in PD pathogenesis. ASN is a major component of Lewy bodies that can be found aggregating in the substantia nigra of individuals with PD. The higher the levels of ASN protein, the more severe the pathology of Lewy bodies that are associated with the symptoms of PD [4]. The accumulation of Lewy bodies consequently leads to the damage of the dopamine cells [2], making the targeting of ASN for inhibition a plausible therapeutic pathway for maintaining dopamine levels and managing PD. Several

treatments targeting the inhibition of the synthesis, aggregation or uptake of abnormal ASN have revealed promising results. However, no inhibitor has yet been approved for clinical usage and further research is required to explore deeper the relationship between ASN and the development of PD [5].

Dopa decarboxylase is an enzyme that converts levodopa to the neurotransmitter, dopamine *via* decarboxylation [2]. It is the main enzyme involved in regulating the amount of dopamine that can reach the brain which greatly affects the development of PD. To regulate the degeneration of dopamine-producing cells, levodopa is usually co-administered with DDC inhibitors to ensure that levodopa reaches the brain before it is converted to dopamine which is impermeable to the blood-brain barrier. A significant amount of levodopa will then reach the nervous system before it is steadily converted to dopamine in the bloodstream. With that, the side effects related to dopamine and the high concentration of levodopa in the bloodstream can be reduced. The administration of levodopa together with DDC inhibitors such as carbidopa and benserazide has been recognized as the most effective symptomatic treatment for PD [6]. However, all these drugs usually display adverse effects especially when it is administered in a high concentration over a long period. For instance, the administration of levodopa causes nausea, vomiting, involuntary movement and orthostatic hypotension whereas the risk of involuntary movements may be increased when carbidopa is co-administered with levodopa [2]. Besides, the co-administration of benserazide with levodopa could also result in adverse effects such as postural hypotension, dyskinesias and psychiatric effects [7]. These make a continuous search for inhibitors of ASN and DDC with improved efficacy and safety remains crucial.

Tetrahydro-β-carboline and carbazole are chemical scaffolds consisting of a tricyclic heterocycle usually synthesized from indole moieties. They are vastly available in natural products and represent medical compounds with diverse pharmacological applications due to their interesting chemical and structural interactions with various biological targets. As such, they are renowned with broad-spectrum activities against cancer, neuropsychiatric disorders, analgesic, anti-inflammation and recently coronavirus 2019 (COVID-19) [8,9]. These confer the scaffolds as worthy of further exploration for potential anti-PD candidates as demonstrated in this study. Moreover, multitarget (one-drug-dual-target) screening through the computational molecular docking analysis not only reduces the cost and resources required for experiments but also enhances the probable strategy for minimizing additive side effects caused by the administration of 2 separate drugs. It is of utmost importance that the compounds identified have minimal side effects and toxicity. As such, *in silico* predictions of ligands under probe for biomedical applications are economical and time-saving for the preliminary evaluation of a promising candidate for further rigorous experimental validation.

Thus, this study aims to discover new potential drug candidates that can inhibit both ASN and DDC responsible for PD from the databases of tetrahydro-β-carboline and carbazole (THBC) derivatives. The screened ligands were further predicted for pharmacokinetics and pharmacodynamics profiles for absorption, distribution, metabolism, excretion and toxicity (ADMET) using pkCSM server.

Materials and methods

Ligand retrieval and preparation

Firstly, the chemical structures of the 270 in-house THBC derivatives databases were drawn in 2D and retrieved in SMILE format using ChemDraw Pro 20.1.1. The molecular structures of the 3 selected ligands were illustrated and the remaining ligands were available in supplementary material (**Figure S1**). The 3D structures of the reference drugs including anle138b, phenylbutyrate, levodopa, benserazide and carbidopa were retrieved from the PubChem database in SDF formats. The retrieved in-house THBC databases and reference drugs were uploaded to the workspace of Maestro 12.2 for ligand preparation using the LigPrep module (LigPrep, Schrodinger, LCC, New York, NY, 2019). All the settings were kept at default except the option of determination of chiralities from the 3D structure was selected. Preparation was achieved through protonation and energy minimization using the OPLS-3e force field. The Epik was used at default settings and the possible ionization states were generated at pH 7.0 ± 2.0 [10]. Finally, the prepared ligand conformers were saved in the LigPrep-out file and ready to be docked.

Protein structure retrieval, preparation and generation of glide-grid box

The crystal structures of human alpha-synuclein (1 - 19) in complex with maltose-binding protein (MBP) (PDB 3Q25) and DDC in complexed with an inhibitor, carbidopa (PDB 1JS3) were retrieved from the RCSB protein data bank in PDB formats [11]. The structures were uploaded to the workspace of Maestro 12.2 and prepared using the protein preparation wizard (Protein Preparation, Schrodinger, LCC, New York, NY, 2019). The preparation processes involve filling in missing side chains and missing loops.

Review and modification were done on ASN and DDC receptors to further remove unwanted chains, water molecules and ions. They were then refined by the process of optimization and minimization. The generation of the receptor grid defines the location of the active pocket in which the ligand binds. The crystal structure of ASN was analyzed by selecting the centroid of the workspace ligand to generate the enclosing glide-grid box for docking. The x, y and z coordinates of 4.77, 29.86 and 7.54 Å respectively and ligands with a length of 20 Å within a cavity volume of 10 Å ×10 Å ×10 Å were obtained for ASN (PDB 3Q25). Similarly, the crystal structure of DDC co-crystallized with carbidopa (PDB 1JS3) was analyzed in the same way to generate the enclosing grid box for docking. The x, y and z coordinates of 43.37, 37.04 and 67.09 Å respectively and ligands with a length of 20 Å within a cavity volume of 10 Å ×10 Å ×10 Å were obtained. The glide grid boxes of both ASN and DDC were saved in the zip file as described in relevant previous studies [9,12].

Molecular docking

The ligand-receptor docking analysis was performed to virtually assess the inhibitory interactions of the prepared ligand conformers against the ASN and DDC receptors. The ligands and reference drugs output files together with the receptor grid zip file were imported into the workspace of the glide. Virtual screening was done using the SP molecular docking modules of Maestro 12.2 (Ligand docking, Schrodinger, LCC, New York, NY, 2019). The docked molecules were ranked accordingly in decreasing order of the docking scores which represent the binding affinity of the ligands towards the receptors. The hydrophilic, electrostatic and hydrophobic interactions of the ligands and reference drugs in the active binding pocket of protein receptors were analyzed using the 2D and 3D binding poses viewed in ligand interaction diagrams. The docking protocols were validated by using the crystal structure of ASN (PDB 3Q25) co-crystallized with the ligand, alpha-maltose (**Figure 1**) [11]. The receptor grid of PDB 3Q25 was generated to locate the binding pocket which binds with the co-crystallized ligand. After ligand preparation using the LigPrep module, alpha-maltose was docked against the prepared receptor grid of PDB 3Q25. The redocked of alpha-maltose within the active pocket of ASN was then superimposed with the original ligand in the crystal complex downloaded from the RCSB protein data bank to calculate the root mean square deviation (RMSD). The value of ≤ 2.0 Å (the smaller the better) indicates that the docking protocols are precise and accurate [13,14].

Prediction of ADMET properties

The pkCSM, a freely accessible server-based tool was used to predict the physicochemical, pharmacokinetics, pharmacodynamics and toxicological properties of the selected ligands and references in terms of ADMET. These were to identify potential drug candidates which can be bound to the protein targets in optimal concentrations, metabolized and absorbed by the body with minimal toxicity whilst producing therapeutic effects. The pkCSM was operated by inputting the SMILES format of all the ligands and references. The parameters for ADMET include molecular weight (MW), lipophilicity (Log P), number of rotatable bonds, hydrogen bond acceptors (HBA), hydrogen bond donors (HBD), solubility (Log S) and topological polar surface area (TPSA). The other parameters such as the potential for blood-brain barrier (BBB), human intestinal absorption, P-glycoprotein substrate, and inhibitory expressions on the cytochrome P450 isoenzymes were determined to identify the druggability of the selected ligands against the protein targets. The parameters were evaluated using the reference of Lipinski's Rules of 5 (RO5) [15]. The ligands which showed good physicochemical, pharmacokinetics, pharmacodynamics and toxicological properties were selected as finally screened ligands amenable for further studies.

Results and discussion

Molecular docking

Molecular docking simulation was done to virtually screen the 379 minimized conformers produced from the preparation of 270 THBC ligands as well as the reference drugs against ASN and DDC. The result for the docking validation showed high similarity in the binding interaction of the redocked ligand and the co-crystallized ligand with ASN (PDB 3Q25) indicated by the glide RMSD value of 0.4642 Å, validating the docking procedures as good and reproducible (**Figure 1**) [10].

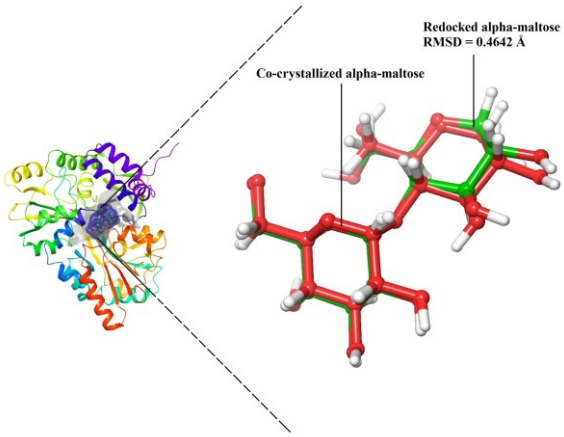

Figure 1 Validation of docking protocols. 3D binding poses of co-crystallized and redocked alpha-maltose superimposed at the active binding pocket of ASN (PDB 3Q25). Ball and stick model: co-crystallized alpha-maltose (red); redocked alpha-maltose (green); RMSD = 0.4642 Å.

It correctly defines the accurate pose of the ligands in the active pocket of the crystal structure of ASN. The SP glide gscores and binding interactions of the top 3 ligands as well as the positive references for ASN and DDC were presented in **Table 1**. Relevant reference drugs such as levodopa, carbidopa, phenylbutyrate, benserazide and anle138b were annotated as R1, R2, R3, R4 and R5 respectively. According to the results, ligands 172, 082 and 013 consistently displayed higher binding affinities in terms of SP glide gscores of –9.154, –9.124, –8.971 kcal/mol against ASN and –6.758, –5.212 and –6.271 kcal/mol against DDC, respectively. Further results of the remaining ligands that docked with ASN and DDC were available in supplementary material (**Table S1**). Most of the ligands showed higher SP glide gscores than R1 and R3 whose SP glide gscores are –8.208 and –7.181 kcal/mol against ASN, and –4.217 and –4.576 kcal/mol against DDC respectively. These support the selected ligands as putative inhibitors of ASN and DDC with strong inhibitory interactions amenable for anti-PD therapeutic design.

From the results (**Table 1**), the ligands expressed strong pharmacological interactions with amino acid residues within the active pocket of ASN and DDC which were illustrated in 2D and 3D interaction diagrams (**Figures 2** and **3**). The binding interactions could enhance the stability of the complex which ideally constitute the inhibitory effects of the ligands against ASN to alleviate the effect of ASN fibrillation. The active binding pocket of the co-crystallized ASN comprised of amino acid residues such as Glu112, Trp231, Asn13, Asp15, Lys16, Phe157, Tyr156, Pro155, Glu154, Trp341, Trp63, Ala64, Asp66, Arg67 and Met331. According to the supporting literature of ASN (PDB 3Q25), the segments that will form fibers were located in the extended loops and coils which were predicted to be at residues 14 - 19, 35 - 42, 47 - 57 and 67 - 72 of the first 72 residues of ASN traced [16]. The structural flexibility of ASN was determined by the formation of loops and turns at the amino acid residues of 14 - 19 and 35 - 72. Ligand 172 with the highest SP glide gscore showed hydrogen bond interaction with Glu154, π-cation interaction with Trp63 and π-π interaction with Tyr156 and Trp341 within the active binding pocket of ASN. Consistently, the top 3 ligands also showed binding interactions with similar amino acid residues that interacted with R3 and R5 such as Asp15, Trp63, Arg67 and Trp341 which have contributed to the high SP glide gscores. These demonstrate the potentials of the selected ligands to inhibit ASN strongly or more as the referenced inhibitor in clinical trials, **R3.**

Against the crystal structure for DDC, all ligands commonly interacted with Trp71, Ala148, Ser149, Hie192, Thr246, Asp271 and Lys303 which are essential amino acid residues at the active site of DDC. From the results (**Table 1**), ligand 172 with the highest SP glide gscore showed interactions with Thr246 through hydrogen bond, Lys303 through π-cation interaction and Hie192 through π-π stacking. Most of the selected ligands interacted with highly conserved residue in the sequences of PLP-dependent decarboxylases crucial for catalytic activity, Hie192 through π-π stacking [6]. Interactions of the ligand 172 with the active residues could promote a stable binding against the active pocket of DDC through Hie192 and other relevant residues. According to the supporting literature of DDC crystal file (PDB 1JS3), the anti-Parkinson drug, R2 is reportedly bound to the receptor through the formation of hydrazone linkage with the cofactor PLP and its catechol ring was buried deeply in the active site pocket of DDC [6]. The top 3 ligands including 172, 082 and 013 showed binding interaction with similar amino acid residues that interacted with R1, R2 and R4 such as Ala148, Ser149, Hie192, Thr246, Hie302 and Lys303 through various

pharmacophores supported by their THBC scaffolds. These potentiate the selected ligands as promising inhibitors of DDC worthy of further exploration in quest for effective anti-PD.

Table 1 Glide gscores and interactions of selected ligands and references with ASN and DDC.

Ligands	ASN (3Q25)					DDC (1JS3)				
	SP glide gscore (kcal/mol)	Interactions				SP glide gscore (kcal/mol)	Interactions			
		Hydrogen bond	Salt bridge	π-cation	π - π		Hydrogen bond	Salt bridge	π-cation	π - π
172	–9.154	Glu154	-	Trp63	Tyr156, Trp341	–6.758	Thr246	-	Lys303	Hie192
082	–9.124	Glu45	Asp66	Arg67, Trp341	Tyr156	–5.212	-	-	Lys303	Trp71, Hie192
013	–8.971	Asp15, Lys16, Asn151	-	-	-	–6.271	Ala148, Ser149, Hie302	-	Lys303	Hie192
R1	–8.208	Lys16, Trp63, Asp66, Arg67, Glu112	Asp66, Arg67	-	-	–4.217	Ala148, Ser149, Asp271, Hie302	Lys303	-	Hie192
R2	–7.458	Trp63, Asp66, Arg67, Glu112	Asp66, Arg67	-	Tyr156	–4.502	Thr246, Asp271, Hie302	Lys303	-	Hie192
R3	–7.181	Trp63, Arg67	Arg67	-	Trp63	–4.576	Ala148, Asn300	Lys303	-	Hie192
R4	–6.001	Asp15, Lys16, Glu45, Glu154	Glu45, Glu46, Glu154	-	-	–4.18	Ala148, Asp271, Hie302	-	-	Hie192
R5	–5.875	Asp15	-	-	Tyr211, Trp341	–4.067	-	-	-	Hie192

Note: R1: Levodopa; R2: Carbidopa; R3: Phenylbutyrate; R4: Benserazide; R5: Anle138b.

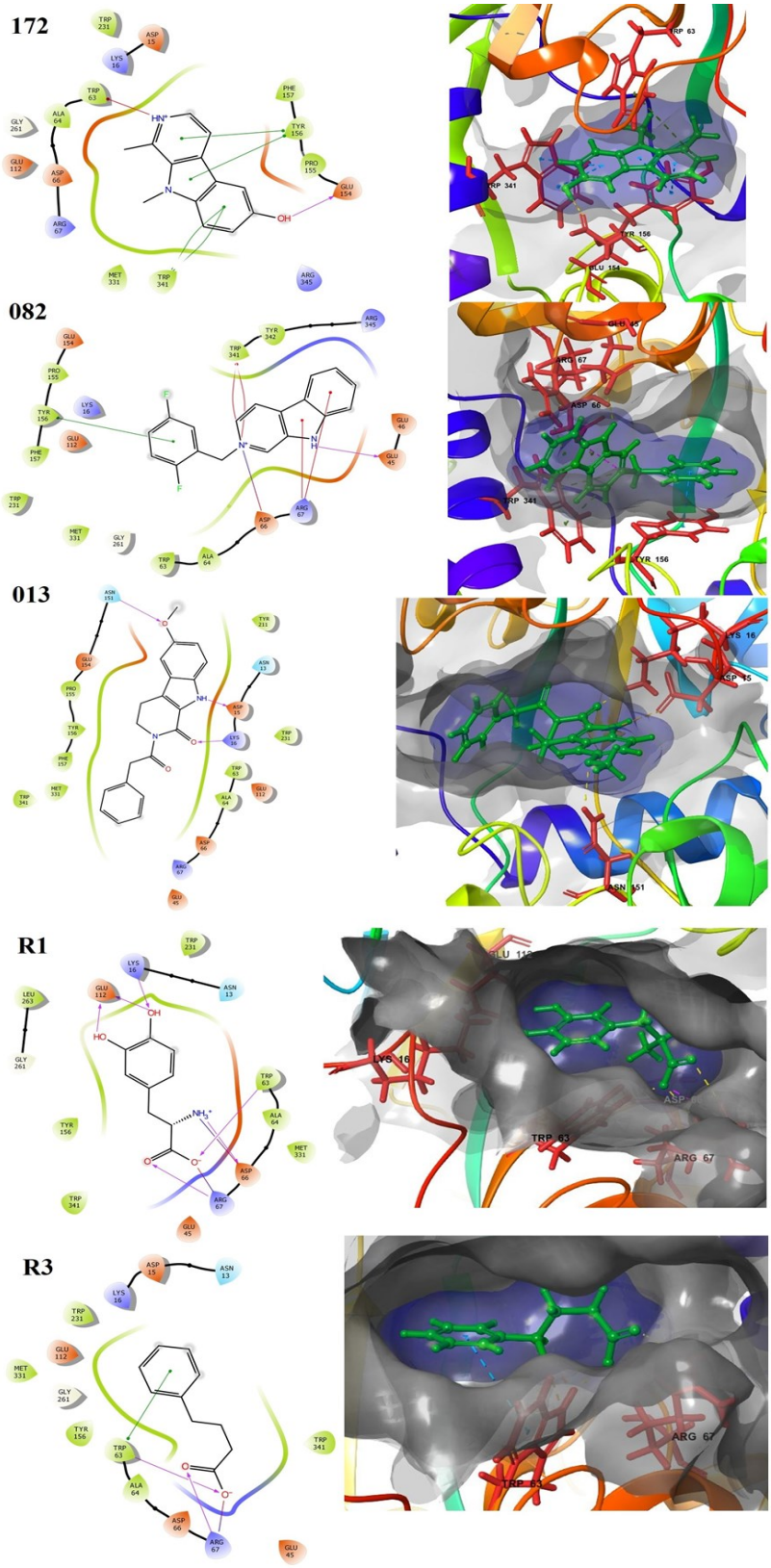

Figure 2 2D and 3D binding poses of the 3 selected ligands and 2 reference drugs with the amino acid residues in the active pocket of ASN using SP molecular docking modules: 2D interaction between ligands and residues are shown as hydrogen bonding (magenta arrow), π-cation (red line), π-π (green line) and salt bridge (red-blue line).

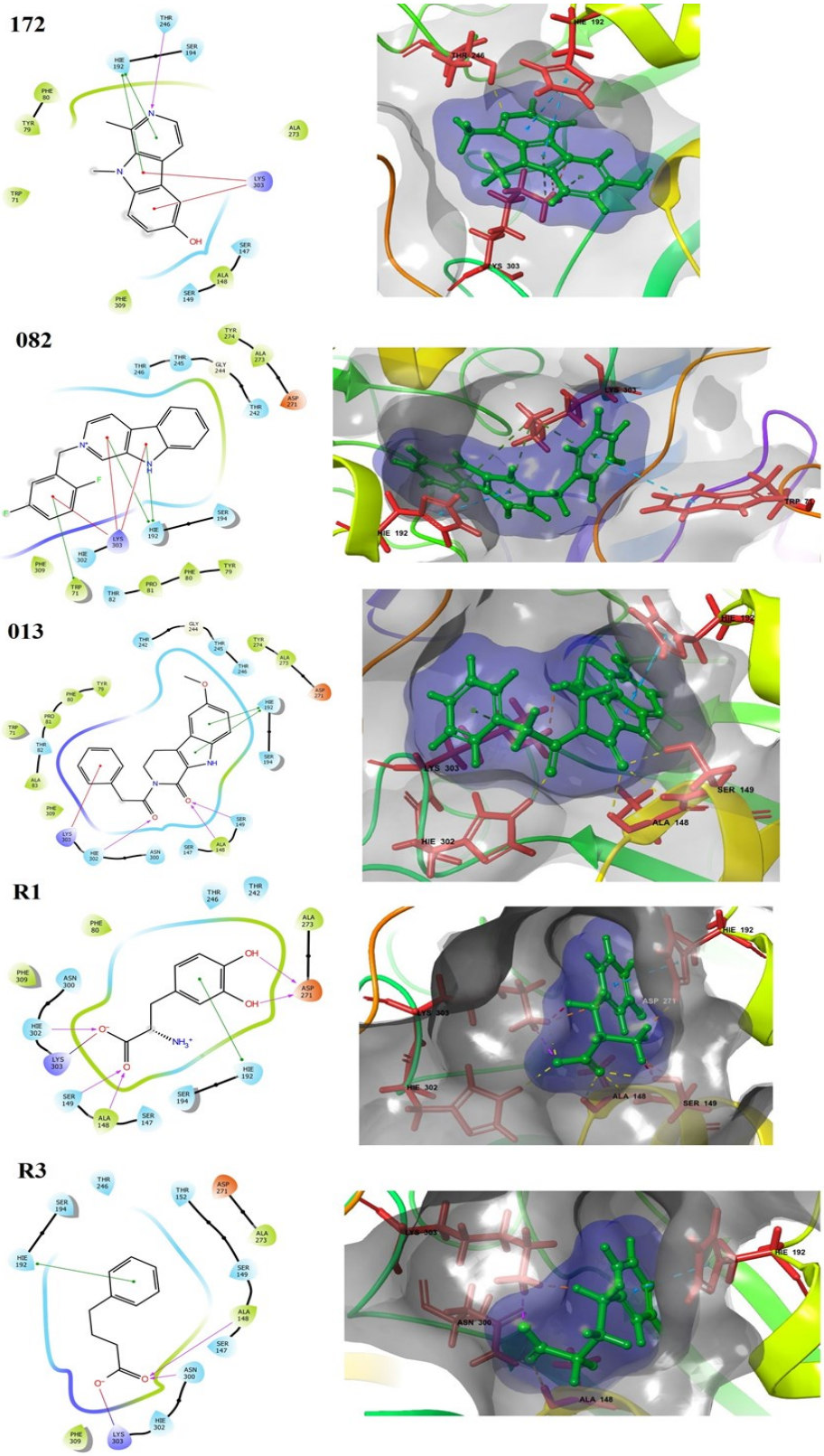

Figure 3 2D and 3D binding poses of the 3 selected ligands and 2 reference drugs with the amino acid residues in the active pocket of DDC using SP molecular docking modules: 2D interaction between ligands and residues are shown as hydrogen bonding (magenta arrow), π-cation (red line), π-π (green line) and salt bridge (red-blue line).

Physicochemical, pharmacokinetics, pharmacodynamics and toxicological properties predictions

The physicochemical, pharmacokinetics, pharmacodynamics and toxicological properties of the selected ligands and references were predicted in terms of ADMET to identify the potential inhibitors of ASN and DDC for PD. The predicted physicochemical parameters of the top 3 ligands selected from the docking studies and references are presented in **Table 2**. Further results of the remaining ligands are available in the supplementary material (**Table S2**). In Lipinski's Rule of 5 (RO5) which was commonly used as a benchmark, a potential drug candidate is expected to have MW of < 500 g/mol, < 10 HBA, < 5 HBD and Log P < 5 for ideal absorption and permeation [15]. Among the 3 ligands, only ligand 172 obeyed the RO5 unlike ligands 082 and 013 which presented TPSA > 130 $Å^2$. As a result, ligands 082 and 013 may have low bioavailability and absorption across the small intestine [17]. High log P value indicates high lipophilicity, denoting that all selected ligands may have potential BBB penetration [18]. However, it is crucial that the potential drug candidate targeting DDC do not cross the BBB, similar to the mechanism initiated by the renowned drug, R2 that inhibits DDC peripherally to allow more metabolism of L-Dopa into dopamine in the CNS [19].

Again, ligands 172 and 082 were predicted to be slightly soluble while ligand 013 was likely insoluble [20]. Although, ligands 172 and 082 have low solubility which may indicate poor absorption, bioavailability and insufficient solubility for intravenous drug administration [21]. However, they have similar results in regards with all reference drugs, indicating less relevance of such properties to anti-PD pharmacology. Furthermore, all of them have a higher Caco2 permeability and percentage of intestinal absorption than R1, R2 and R4, hypothetically for higher permeability and absorption across human epithelial colorectal adenocarcinoma cells and intestinal cells. Moreover, all ligands and references expressed the potential as P-gp substrate except R2, R3 and R4. Therefore, they have the ability to protect the CNS from xenobiotics and reduce the toxicity resulting from drug-drug interactions [22,23]. However, at the same time, P-gp substrate decreases the absorption, oral bioavailability and retention time of drugs at the target site [24], a concern for further study. Accordingly, the predicted inhibition of P-gp I and II by ligands 013 and 082 respectively could improve the drug bioavailability and absorption [24].

The cytochromes P450 (CYP) superfamily comprising of CYP1A2, CYP2C19, CYP2C9, CYP2D6 and CYP3A4 are important in the metabolism and detoxification of drugs, thereby protecting the body tissues from damage [25]. Only ligand 082 showed potential as the substrates for both CYP2D6 and CYP3A4 whereas ligand 013 showed potential as a substrate for CYP3A4. CYP450 substrates were able to increase the synthesis and activity of enzymes [25]. Ligand 172 has the least potential to act as the inhibitor of the CYP superfamily isoenzymes. Therefore, this ligand most likely will not result in the undesired drug-drug interactions leading to toxicity caused by the accumulation of drugs in the body [22].

Among the 3 ligands, only ligand 013 did not show AMES toxicity that is associated with mutagenic potential. Furthermore, ligand 172 did not display potential as inhibitors of the potassium channels encoded by hERG I and II. Moreover, all ligands did not result in hepatotoxicity except ligand 013. Although, drug candidates that did not result in hepatotoxicity could still be applicable as anti-Parkinson drugs, similarly to R1, R2, R3 and R5 which showed positive results in hepatotoxicity. Finally, all the ligands showed LC_{50} values of > –0.3 log mM which were identified as having lower acute toxicity than R5.

Overall, from the predictions of pkCSM for different parameters of ADMET, ligand 172 was found to be the most putative compound which could be selected as the drug candidate. The ligand has 0 violation for the Lipinski's RO5, higher Caco2 permeability, intestinal absorption and BBB permeability than R1, R2 and R4, higher CNS permeability than almost all references, low potentials for hERG I and II inhibition, no hepatotoxicity, skin sensitization and Minnow toxicity. The results boost the overall potentials of the selected ligands (**Figure 4**), especially 172 as promising candidate for PD with enhanced pharmacological and safety profiles adequately enough for replacing some of the current anti-PD medications. However, further analysis through experimental studies is required to validate the results.

Table 2 Predicted ADMET properties of the selected ligands and references.

Properties	Descriptors	172	082	013	R1	R2	R3	R4	R5
MW	(g/mol)	212.252	375.216	334.375	197.19	226.232	164.204	257.246	343.18
Log P	-	2.74052	0.9391	2.9441	0.0522	–0.0531	2.0939	–1.7562	4.2349
#Rot. bonds	-	0	2	3	3	4	4	5	2
#HBA	-	3	0	3	4	5	1	7	3
#HBD	-	1	1	1	4	5	1	7	1
TPSA	$(Å)^2$	92.958	141.699	144.76	80.41	92.295	71.847	102.639	129.397
Absorption	Solubility (log mol/L)	–2.966	–3.862	–4.288	–2.89	–2.525	–2.836	–2.137	–3.363
Absorption	Caco2 permeability	1.062	1.47	0.913	–0.289	–0.081	1.705	–0.824	1.308
Absorption	Intestinal absorption (%) (human)	95.35	90.958	94.008	47.741	37.165	94.825	36.487	92.057
Absorption	Skin permeability (log Kp)	–2.718	–2.73	–2.986	–2.735	–2.735	–2.695	–2.735	–2.736
Absorption	P-glycoprotein substrate	Yes	Yes	Yes	Yes	No	No	No	Yes
Absorption	P-glycoprotein I inhibitor	No	No	Yes	No	No	No	No	No
Absorption	P-glycoprotein II inhibitor	No	Yes	No	No	No	No	No	Yes
Distribution	VDss (human)	0.367	0.795	0.172	–0.105	–1.134	–0.831	–0.181	0.226
Distribution	Fraction unbound (human)	0.337	0.297	0	0.604	0.697	0.29	0.961	0.073
Distribution	BBB permeability	0.341	–0.31	–0.103	–0.843	–1.02	0.354	–1.45	0.353
Distribution	CNS permeability	–1.771	–1.574	–2.138	–3.032	–3.234	–1.854	–4.467	–1.157
Metabolism	CYP2D6 substrate	No	Yes	No	No	No	No	No	No
Metabolism	CYP3A4 substrate	No	Yes	Yes	No	No	No	No	No
Metabolism	CYP1A2 inhibitor	Yes	Yes	Yes	No	No	No	No	Yes
Metabolism	CYP2C19 inhibitor	No	No	Yes	No	No	No	No	Yes
Metabolism	CYP2C9 inhibitor	No	No	Yes	No	No	No	No	No
Metabolism	CYP2D6 inhibitor	No	Yes	No	No	No	No	No	Yes
Metabolism	CYP3A4 inhibitor	No	No	Yes	No	No	No	No	Yes
Excretion	Total clearance (log mL/min/kg)	0.624	1.407	0.256	0.43	0.499	0.349	0.873	0.13
Excretion	Renal OCT2 substrate	No	No	No	No	No	No	No	No
Toxicity	AMES toxicity	Yes	Yes	No	No	No	No	No	No
Toxicity	Max. tolerated dose (log mg/kg/day)	0.438	–0.047	0.267	0.922	0.673	0.923	0.637	0.549
Toxicity	hERG I inhibitor	No	No	No	No	No	No	No	No
Toxicity	hERG II inhibitor	No	Yes	Yes	No	No	No	No	Yes
Toxicity	Oral Rat Acute Toxicity (LD50) (mol/kg)	2.687	2.712	1.996	2.234	2.72	2.077	2.211	2.757

Properties	Descriptors	172	082	013	R1	R2	R3	R4	R5
Toxicity	Oral Rat Chronic Toxicity (LOAEL) (log mg/kg/day)	1.355	1.56	1.438	2.699	2.155	2.731	3.799	1.185
Toxicity	Hepatotoxicity	No	No	Yes	Yes	Yes	Yes	No	Yes
Toxicity	Skin Sensitization	No	No	No	No	No	Yes	No	No
Toxicity	T. Pyriformis toxicity (log µg/L)	0.599	0.312	0.644	0.281	0.285	0.347	0.285	0.343
Toxicity	Minnow toxicity (log mM)	0.259	0.197	0.283	3.143	3.196	1.243	4.246	–1.408

Note: R1: Levodopa; R2: Carbidopa; R3: Phenylbutyrate; R4: Benserazide; R5: Anle138b; MW = Molecular weight; HBA = H-bond acceptor; HBD = H-bond donor; TPSA = Topological polar surface area.

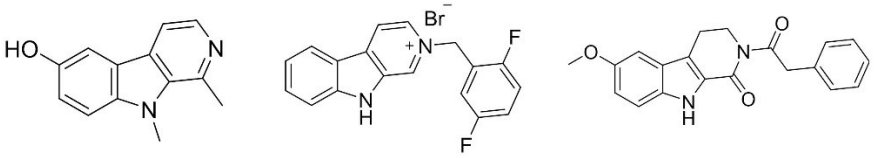

Ligand 172 **Ligand 082** **Ligand 013**

Figure 4 Molecular structures of the selected THBC ligands as potent inhibitors of ASN and DDC.

Conclusions

This study involves the application of computational molecular docking software and server-based tools such as pkCSM to evaluate the binding affinities, and physicochemical and drug-like properties of 270 THBC ligands against the ASN and DDC protein targets in comparison with 5 references, levodopa, carbidopa, phenylbutyrate, benserazide and anle138b. The results from the molecular docking and predicted ADMET parameters are important determinants that could aid further studies of the ligands as promising candidates for PD, targeting the ASN and DDC. The potential ligands identified with stronger inhibitory interactions than the references can be tested in experimental study to evaluate their functions and effects during administration. The discovery of multitarget inhibitors will be beneficial as it cuts down on the cost and resources used during the early stage of research and reduces the side effects and toxicity caused by the administration of multiple drugs to inhibit different relevant targets. Finally, the study demonstrates a successful application of computer-aided method of drug design for speedy identification of potential candidates for PD in an environmentally friendly manner.

Acknowledgements

This work was partly supported by Fundamental Research Grant, Ministry of Higher Education, Malaysia (grant no. 203.CDADAH.6711955) and sponsorship from Jabatan Perkhidmatan Awam (JPA). TXY is thankful to the Centre for Drug Research, Universiti Sains Malaysia for the internship opportunity.

References

[1] F Daidone, R Montioli, A Paiardini, B Cellini, A Macchiarulo, G Giardina, F Bossa and CB Voltattorni. Identification by virtual screening and *in vitro* testing of human DOPA decarboxylase inhibitors. *PLos One* 2012; **7**, e31610.

[2] JT Boyd, C English and KM Lounsbury. 13 - Antiparkinson drugs. *Pharmacol. Therapeut. Dent.* 2017; **2017**, 193-205.

[3] Z Ou, J Pan, S Tang, D Duan, D Yu, H Nong and Z Wang. Global trends in the incidence, prevalence, and years lived with disability of Parkinson's disease in 204 countries/territories from 1990 to 2019. *Front. Publ. Health* 2021; **9**, 776847.

[4] HG Jasutkar, SE Oh and MM Mouradian. Therapeutics in the pipeline targeting α-synuclein for Parkinson's disease. *Pharmacol. Rev*. 2022; **74**, 207-37.

[5] CR Fields, N Bengoa-Vergniory and R Wade-Martins. Targeting alpha-synuclein as a therapy for Parkinson's disease. *Front. Mol. Neurosci.* 2019; **12**, 299.
[6] P Burkhard, P Dominici, C Borri-Voltattorni, JN Jansonius and VN Malashkevich. Structural insight into Parkinson's disease treatment from drug-inhibited DOPA decarboxylase. *Nat. Struct. Biol.* 2001; **8**, 963-7.
[7] JA Davies. *Benserazide*. *In*: xPharm: The comprehensive pharmacology reference. Elsevier, Netherlands, 2007.
[8] YO Ayipo, MN Mordi, M Mustapha and T Damodaran. Neuropharmacological potentials of β-carboline alkaloids for neuropsychiatric disorders. *Eur. J. Pharmacol.* 2021; **893**, 173837.
[9] YO Ayipo, I Ahmad, YS Najib, SK Sheu, H Patel and MN Mordi. Molecular modelling and structure-activity relationship of a natural derivative of o-hydroxybenzoate as a potent inhibitor of dual NSP3 and NSP12 of SARS-CoV-2: *In silico* study. *J. Biomol. Struct. Dynam.* 2023; **41**, 1959-77.
[10] YO Ayipo, WA Alananzeh, SN Yahayaa and MN Mordi. Molecular modelling and virtual screening to identify new piperazine derivatives as potent human 5-HT1A antagonists and reuptake inhibitors. *Combin. Chem. High Throughput Screen.* 2022, https://doi.org/10.2174/1386207325666220524094913
[11] SK Burley, C Bhikadiya, C Bi, S Bittrich, L Chen, GV Crichlow, CH Christie, K Dalenberg, LD Costanzo, JM Duarte, S Dutta, Z Feng, S Ganesan, DS Goodsell, S Ghosh, RK Green, V Guranović, D Guzenko, BP Hudson, CL Lawson, ..., M Zhuravleva. RCSB protein data bank: Powerful new tools for exploring 3D structures of biological macromolecules for basic and applied research and education in fundamental biology, biomedicine, biotechnology, bioengineering and energy sciences. *Nucleic Acids Res.* 2021; **49**, D437-51.
[12] YO Ayipo, WA Alananzeh, I Ahmad, H Patel and MN Mordi. Structural modelling and *in silico* pharmacology of β-carboline alkaloids as potent 5-HT1A receptor antagonists and reuptake inhibitors. *J. Biomol. Struct. Dynam.* 2022, https://doi.org/10.1080/07391102.2022.2104376.
[13] A Castro-Alvarez, AM Costa and J Vilarrasa. The performance of several docking programs at reproducing protein-macrolide-like crystal structures. *Molecules* 2017; **22**, 136.
[14] D Ramírez and J Caballero. Is it reliable to take the molecular docking top scoring position as the best solution without considering available structural data? *Molecules* 2018; **23**, 1038.
[15] CA Lipinski, F Lombardo, BW Dominy and PJ Feeney. Experimental and computational approaches to estimate solubility and permeability in drug discovery and development settings. *Adv. Drug Deliv. Rev.* 2001; **46**, 3-26.
[16] M Zhao, D Cascio, MR Sawaya and D Eisenberg. Structures of segments of α-synuclein fused to maltose-binding protein suggest intermediate states during amyloid formation. *Protein Sci.* 2011; **20**, 996-1004.
[17] JV Turner and S Agatonovic-Kustrin. *In silico prediction of oral bioavailability*. *In*: Comprehension medicinal chemistry II. Elsevier Science, Naterlands, 2007, p. 699-724.
[18] H Pajouhesh and GR Lenz. Medicinal chemical properties of successful central nervous system drugs. *NeuroRx* 2005; **2**, 541-53.
[19] E Leyden and P Tadi. *Carbidopa*. StatPearls, Florida, 2023.
[20] MC Sorkun, A Khetan and S Er. AqSolDB, a curated reference set of aqueous solubility and 2D descriptors for a diverse set of compounds. *Sci. Data* 2019; **6**, 143.
[21] KT Savjani, AK Gajjar and JK Savjani. Drug solubility: Importance and enhancement techniques. *ISRN Pharmacol*. 2012; **2012**, 195727.
[22] A Daina, O Michielin and V Zoete. SwissADME: A free web tool to evaluate pharmacokinetics, drug-likeness and medicinal chemistry friendliness of small molecules. *Sci. Rep.* 2017; **7**, 42717.
[23] LM Lagares, N Minovski and M Novič. Multiclass classifier for P-glycoprotein substrates, inhibitors, and non-active compounds. *Molecules* 2019; **24**, 2006.
[24] ML Amin. P-glycoprotein inhibition for optimal drug delivery. *Drug Target Insights* 2013; **7**, 27-34.
[25] T Lynch and A Price. The effect of cytochrome P450 metabolism on drug response, interactions, and adverse effects. *Am. Fam. Physician* 2007; **76**, 391-6.

Supplementary material

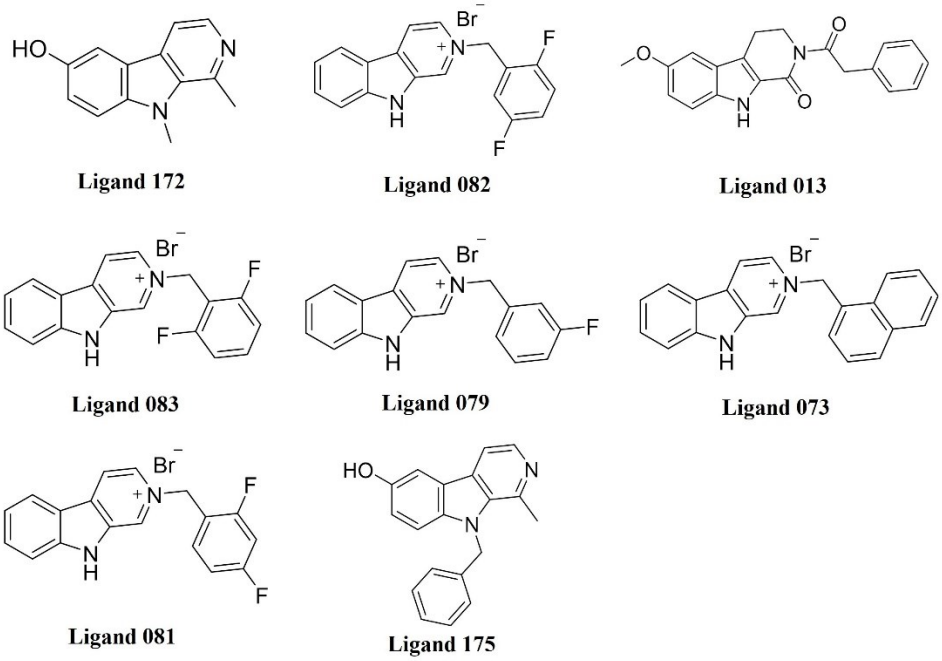

Figure S1 Molecular structures of the top eight selected THBC ligands as potent inhibitors of ASN and DDC.

Table S1 Glide gscores and interactions of the top eight selected ligands and references with Alpha-synuclein (ASN) and Dopa decarboxylase (DDC).

Ligands	ASN (3Q25)					DDC (1JS3)				
	SP (Glide Gscore)	Interactions				SP (Glide Gscore)	Interactions			
		Hydrogen bond	Salt bridge	π-cation	π - π		Hydrogen bond	Salt bridge	π-cation	π - π
172	-9.154	Glu154	-	Trp63	Tyr156, Trp341	-6.758	Thr246	-	Lys303	Hie192
082	-9.124	Glu45	Asp66	Arg67, Trp341	Tyr156	-5.212	-	-	Lys303	Trp71, Hie192
013	-8.971	Asp15, Lys16, Asn151	-	-	-	-6.271	Ala148, Ser149, Hie302	-	Lys303	Hie192
083	-8.728	Glu45	-	Arg67, Trp341	Tyr156, Trp341	-4.885	-	-	Lys303	Hie192
079	-8.612	Glu45	-	Arg67, Trp341	Tyr156	-4.788	-	-	Lys303	Trp71, Hie192
073	-8.606	Glu45	-	Arg67, Trp341	Tyr156	-4.715	-	-	Lys303	Trp71, Hie192
081	-8.566	Glu45	-	Arg67, Trp341	Tyr156	-4.804	-	-	Lys303	Hie192
175	-8.196	Asp15, Glu154	Asp15	Lys16	Tyr156, Phe157	-5.534	-	-	Lys303	Tyr79
R1	-8.208	Lys16, Trp63, Asp66, Arg67, Glu112	Asp66, Arg67	-	-	-4.217	Ala148, Ser149, Asp271, Hie302	Lys303	-	Hie192

Ligands	ASN (3Q25)					DDC (1JS3)				
	SP (Glide Gscore)	Interactions				SP (Glide Gscore)	Interactions			
		Hydrogen bond	Salt bridge	π-cation	π - π		Hydrogen bond	Salt bridge	π-cation	π - π
R2	-7.458	Trp63, Asp66, Arg67, Glu112	Asp66, Arg67	-	Tyr156	-4.502	Thr246, Asp271, Hie302	Lys303	-	Hie192
R3	-7.181	Trp63, Arg67	Arg67	-	Trp63	-4.576	Ala148, Asn300	Lys303	-	Hie192
R4	-6.001	Asp15, Lys16, Glu45, Glu154	Glu45, Glu46, Glu154	-	-	-4.18	Ala148, Asp271, Hie302	-	-	Hie192
R5	-5.875	Asp15	-	-	Tyr211, Trp341	-4.067	-	-	-	Hie192

Hint: **R1**: Levodopa; **R2**: Carbidopa; **R3**: Phenylbutyrate; **R4**: Benserazide; **R5**: Anle138b.

Table S2 Predicted ADMET properties of the selected ligands and references.

Properties	Descriptors	172	082	013	83	79	73	81	175	R1	R2	R3	R4	R5
MW	(g/mol)	212.252	375.216	334.375	375.216	357.226	389.296	375.216	288.35	197.19	226.232	164.204	257.246	343.18
Log P	-	2.74052	0.9391	2.9441	0.9391	0.8	1.8141	0.9391	4.25182	0.0522	-0.0531	2.0939	-1.7562	4.2349
#Rot. bonds	-	0	2	3	2	2	2	2	2	3	4	4	5	2
#HBA	-	3	0	3	0	0	0	0	3	4	5	1	7	3
#HBD	-	1	1	1	1	1	1	1	1	4	5	1	7	1
TPSA	(Å)2	92.958	141.699	144.76	141.699	137.534	156.05	141.699	128.015	80.41	92.295	71.847	102.639	129.397
Absorption	Solubility (log mol/L)	-2.966	-3.862	-4.288	-3.831	-4.656	-5.3	-3.788	-4.017	-2.89	-2.525	-2.836	-2.137	-3.363
Absorption	Caco2 permeability	1.062	1.47	0.913	1.727	1.536	0.75	1.306	1.315	-0.289	-0.081	1.705	-0.824	1.308
Absorption	Intestinal absorption (%) (human)	95.35	90.958	94.008	91.029	87.32	100	91.14	95.022	47.741	37.165	94.825	36.487	92.057
Absorption	Skin permeability (log Kp)	-2.718	-2.73	-2.986	-2.729	-2.731	-2.735	-2.737	-2.73	-2.735	-2.735	-2.695	-2.735	-2.736
Absorption	P-glycoprotein substrate	Yes	Yes	Yes	Yes	Yes	Yes	Yes	Yes	Yes	No	No	No	Yes
Absorption	P-glycoprotein I inhibitor	No	No	Yes	No	No	Yes	No	No	No	No	No	No	No
Absorption	P-glycoprotein II inhibitor	No	Yes	No	Yes	Yes	Yes	Yes	Yes	No	No	No	No	Yes
Distribution	VDss (human)	0.367	0.795	0.172	0.818	0.527	0.3	0.92	0.039	-0.105	-1.134	-0.831	-0.181	0.226
Distribution	Fraction unbound (human)	0.337	0.297	0	0.289	0.258	0.206	0.321	0.23	0.604	0.697	0.29	0.961	0.073
Distribution	BBB permeability	0.341	-0.31	-0.103	-0.269	-0.289	0.776	-0.308	0.376	-0.843	-1.02	0.354	-1.45	0.353
Distribution	CNS permeability	-1.771	-1.574	-2.138	-1.6	-1.407	-0.859	-1.581	-1.448	-3.032	-3.234	-1.854	-4.467	-1.157
Metabolism	CYP2D6 substrate	No	Yes	No	Yes	Yes	No	Yes	No	No	No	No	No	No
Metabolism	CYP3A4 substrate	No	Yes	Yes	Yes	Yes	Yes	Yes	No	No	No	No	No	No
Metabolism	CYP1A2 inhibitor	Yes	Yes	Yes	Yes	Yes	Yes	Yes	Yes	No	No	No	No	Yes
Metabolism	CYP2C19 inhibitor	No	No	Yes	No	No	Yes	No	Yes	No	No	No	No	Yes
Metabolism	CYP2C9 inhibitor	No	No	Yes	No	No	No	No	No	No	No	No	No	No

Properties	Descriptors	172	082	013	83	79	73	81	175	R1	R2	R3	R4	R5
Metabolism	CYP2D6 inhibitor	No	Yes	No	Yes	Yes	Yes	Yes	Yes	No	No	No	No	Yes
Metabolism	CYP3A4 inhibitor	No	No	Yes	No	No	No	No	No	No	No	No	No	Yes
Excretion	Total clearance (log mL/min/kg)	0.624	1.407	0.256	1.384	1.445	1.467	1.428	0.517	0.43	0.499	0.349	0.873	0.13
Excretion	Renal OCT2 substrate	No	No	No	No	No	No	No	No	No	No	No	No	No
Toxicity	AMES toxicity	Yes	Yes	No	Yes	Yes	Yes	Yes	Yes	No	No	No	No	No
Toxicity	Max. tolerated dose (log mg/kg/day)	0.438	-0.047	0.267	-0.064	0.323	0.298	-0.086	0.597	0.922	0.673	0.923	0.637	0.549
Toxicity	hERG I inhibitor	No	No	No	No	No	No	No	No	No	No	No	No	No
Toxicity	hERG II inhibitor	No	Yes	Yes	Yes	Yes	Yes	Yes	Yes	No	No	No	No	Yes
Toxicity	Oral Rat Acute Toxicity (LD50) (mol/kg)	2.687	2.712	1.996	2.737	2.468	2.312	2.718	2.101	2.234	2.72	2.077	2.211	2.757
Toxicity	Oral Rat Chronic Toxicity (LOAEL) (log mg/kg/day)	1.355	1.56	1.438	1.538	-0.055	-0.35	1.562	1.001	2.699	2.155	2.731	3.799	1.185
Toxicity	Hepatotoxicity	No	No	Yes	No	No	Yes	No	No	Yes	Yes	Yes	No	Yes
Toxicity	Skin Sensitisation	No	No	No	No	No	No	No	No	No	No	Yes	No	No
Toxicity	T. Pyriformis toxicity (log µg/L)	0.599	0.312	0.644	0.298	0.392	0.291	0.313	0.322	0.281	0.285	0.347	0.285	0.343
Toxicity	Minnow toxicity (log mM)	0.259	0.197	0.283	0.236	0.484	0.467	-0.217	0.355	3.143	3.196	1.243	4.246	-1.408

Hint: **R1**: Levodopa; **R2**: Carbidopa; **R3**: Phenylbutyrate; **R4**: Benserazide; **R5**: Anle138b; MW= Molecular weight; HBA= H-bond acceptor; HBD= H-bond donor; TPSA= Topological polar surface area.